AIP Applied Physics Letters

Oxygen vacancy controlled tunable magnetic and electrical transport properties of (Li, Ni)-codoped ZnO thin films

E. Senthil kumar, S. Venkatesh, and M. S. Ramachandra Rao

Citation: Applied Physics Letters **96**, 232504 (2010); doi: 10.1063/1.3449122
View online: http://dx.doi.org/10.1063/1.3449122
View Table of Contents: http://scitation.aip.org/content/aip/journal/apl/96/23?ver=pdfcov
Published by the AIP Publishing

Oxygen vacancy controlled tunable magnetic and electrical transport properties of (Li, Ni)-codoped ZnO thin films

E. Senthil kumar,[1] S. Venkatesh,[2] and M. S. Ramachandra Rao[1,a)]
[1]*Department of Physics, Nano Functional Materials Technology Centre and Materials Science Research Centre, Indian Institute of Technology Madras, Chennai 600 036, India*
[2]*Department of Condensed Matter Physics and Material Sciences, Tata Institute of Fundamental Research, Mumbai 400005, India*

(Received 12 April 2010; accepted 19 May 2010; published online 9 June 2010)

We investigated the electrical, magnetic, and magnetotransport properties of Li–Ni codoped ZnO thin films in the electron dominated, hole dominated, and insulating regimes. In a narrow window of oxygen growth pressure, 10^{-3}–10^{-2} mbar, the films exhibited p-type conductivity with a maximum hole concentration $\sim 8.2\times10^{17}$ cm^{-3}. Magnetoresistance exhibited by the films is attributed to scattering of charge carriers due to localized magnetic moments. Insulating films showed superparamagnetic behavior, whereas both n-type and p-type films showed room temperature ferromagnetism. Our findings suggest that oxygen vacancies and Ni ions in cation site are jointly responsible for ferromagnetism that is not dependent on the carrier type. © *2010 American Institute of Physics*. [doi:10.1063/1.3449122]

ZnO has been extensively studied because of its substantial and intriguing properties in the field of transparent electronics, optoelectronics, and dilute magnetic semiconductors.[1–3] The search for p-type conductivity and room temperature ferromagnetism in ZnO are the most active research areas in recent years. It has been shown that p-type conductivity can be realized by codoping of group I or group V elements with a reactive donor and the intriguing results on room temperature ferromagnetism has been shown to be materialized by doping with transition metal (TM) ions in ZnO.[4–6] There have been a lot of literatures on the realization of room temperature ferromagnetism in TM ion doped ZnO, TM ion doped p-ZnO, and even in unintentionally doped ZnO thin films grown by various techniques.[7–12] Nevertheless, the origin of ferromagnetism in ZnO is still an open debate, i.e., whether the ferromagnetism is an intrinsic property of the material or does it arise from the dopant clusters. It has been theoretically predicted by Dietl that room temperature ferromagnetism can be achieved in Mn doped p-ZnO.[11] However, Sato *et al.*[13] reported room temperature ferromagnetism in Co doped ZnO with n-type doping. On the contrary, Coey's group[14,15] reported the role of oxygen vacancies to obtain ferromagnetism in ZnO and other oxide systems. Recent reports also show that oxygen vacancies play a key role in controlling p-type conductivity and ferromagnetism in ZnO.[16–18] When compared with the Co or Mn doped ZnO thin films, reports on systematic transport studies are scarce in Ni doped ZnO thin films. In particular, we hardly find any experimental report on the transport studies in Li–Ni codoped ZnO thin films. Hence, in this paper we have made a systematic effort to carry out electrical, magnetic, and magnetotransport studies in the n-type, p-type, and insulating regimes to understand the origin of ferromagnetism, if any, in ZnO.

$Zn_{0.96}Li_{0.02}Ni_{0.02}O$ thin films with a thickness of 300 nm were grown on c-sapphire substrates at 400 °C with an oxygen pressure varying from 3.5×10^{-5} to 0.35 mbar using pulsed laser deposition [Neodymium doped Yttrium Aluminium Garnet (Nd:YAG) laser, $\lambda=355$ nm operated at 10 Hz with a laser fluency ~ 2.7 J cm^{-2}]. The films were characterized by x-ray diffraction and x-ray photoelectron spectroscopy (XPS) for structural and valence state analysis, respectively. Electrical resistivity, Hall effect, and magnetoresistance (MR) measurements were performed using physical property measurement system (PPMS, Quantum Design, USA). Magnetization measurements were carried out using Quantum Design SQUID—vibrating sample magnetometer.

Figure 1(a) shows the XRD (θ-2θ) plots of the Li–Ni codoped ZnO thin films grown at different oxygen pressures. All the films showed preferential c-axis (00*l*) orientation of the wurtzite ZnO. No secondary and metallic Ni peaks were observed in any of the films. Figures 1(b) and 1(c) show the XPS results of the film grown at 0.035 mbar. It is found that the O 1*s* level consists of two peaks, O_I and O_{II}, centered at 532.43 eV and 530.99 eV, respectively. The former corresponds to surface oxygen states and the later corresponds to oxygen vacancies. Ni $2p_{3/2}$ level consists of two peaks centered at 853.63 eV and 855.74 eV corresponding to Ni^{2+} and Ni^{3+} chemical states, respectively. We did not observe any metallic Ni peak in the spectra indicating that there has been no Ni segregation in the film.

Figure 2(a) shows the temperature dependent electrical resistivity (ρ) of the Li–Ni codoped ZnO thin films grown at different oxygen partial pressures. All the films show typical semiconducting behavior with activated band conduction at high temperatures ($T>200$ K) and variable range hopping (VRH) conduction at low temperatures. A linear fit of three-dimensional VRH, ln ρ versus $T^{-1/4}$, is shown in Fig. 2(b). Figure 2(c) gives the room temperature electrical transport properties of the Li–Ni codoped ZnO thin films as a function of oxygen growth pressure. We have observed three interesting conductivity regimes. The films grown at oxygen pressure in the range 10^{-5} and 10^{-4} mbar show n-type conductivity and exhibited electron concentrations $\sim 3.2\times10^{18}$–2.4×10^{17} cm^{-3}. The films grown at 10^{-1} mbar and

a)Electronic mail: msrrao@iitm.ac.in.

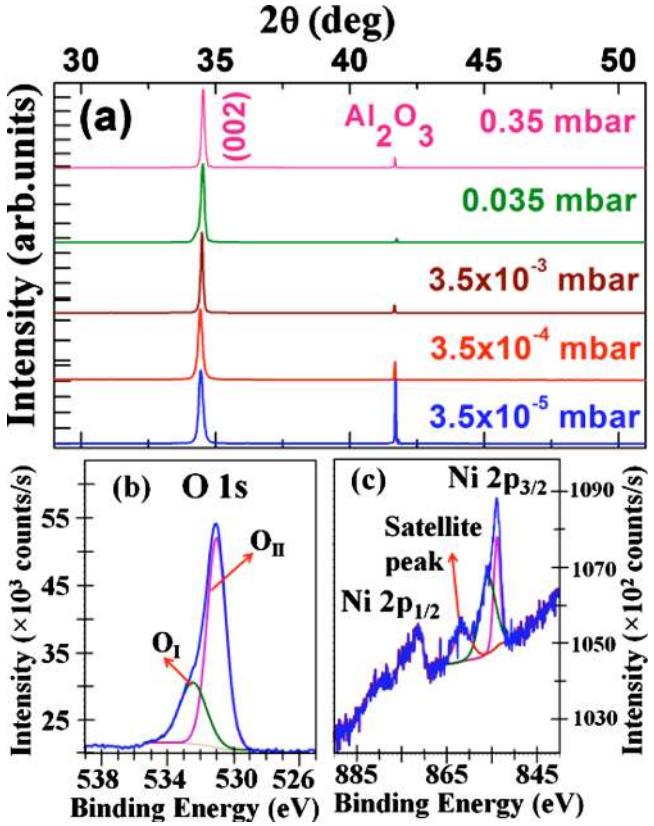

FIG. 1. (Color online) (a) XRD patterns of the Li–Ni codoped ZnO thin films grown at various oxygen pressure. [(b) and (c)] XPS spectra of the Li–Ni codoped ZnO thin film grown at 0.035 mbar depicting O 1*s* and Ni 2*p* levels, respectively.

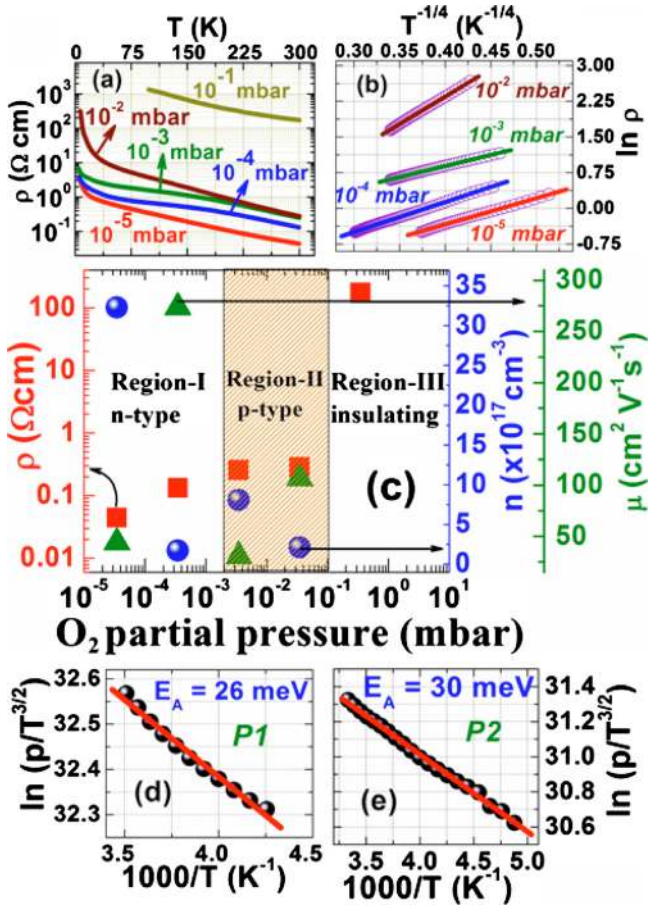

FIG. 2. (Color online) Electrical transport properties of Li–Ni codoped ZnO thin films (a) temperature dependent electrical resistivity, (b) VRH, ln (ρ) vs $T^{-1/4}$, and (c) room temperature electrical transport properties as a function of oxygen partial pressure. [(d) and (e)] Linear fit to $\ln(p/T^{3/2})$ vs $1/T$ of *P*1 and *P*2 thin films, respectively.

above show insulating behavior and because of the high resistivity of these films, Hall effect measurements could not performed on these insulating films. However, we observed an interesting narrow window of growth pressure between 10^{-3} and 10^{-2} mbar, in which the films showed stable p-type conduction. Variation in Hall voltage with the magnetic field with a positive slope and clear rectifying characteristics of p-ZnO/n-Si p-n junction unequivocally confirm the p-type behavior (not shown). Hereafter, the films grown at 10^{-5}, 10^{-4}, 10^{-3}, 10^{-2}, and 10^{-1} mbar will be referred as *N*1, *N*2, *P*1, *P*2, and *I*, respectively. The films *P*1 and *P*2 show hole concentration $\sim 8.2\times10^{17}$ cm^{-3} and 2.4×10^{17} cm^{-3}, respectively, at room temperature. The acceptor activation energy of the p-type films can be derived from the relation,[5] $p \propto T^{3/2} \exp(-E_A/k_B T)$, where, k_B is the Boltzmann's constant and T is the absolute temperature. Figures 2(d) and 2(e) show the linear fit, $\ln(p/T^{3/2})$ versus $1/T$, from which the hole activation energy E_A has been calculated as 26 meV and 30 meV for the films *P*1 and *P*2, respectively.

Figures 3(a)–3(d) show the MR as a function of the applied magnetic field of the samples *N*1, *N*2, *P*1, and *P*2, respectively. The %MR was calculated using the relation $\%MR=\{[R(H)-R(0)]/R(0)\}\times100$, where $R(H)$ is the resistance of the sample in an applied magnetic field, H, and $R(0)$ is the resistance at zero magnetic field. At $H=80$ kOe, samples *N*1, *N*2, and *P*1 showed a maximum negative MR $\sim$15.8%, 14.7%, and 12.6%, respectively, at 5 K. Sample *P*2, for which MR could not be measured at 5 K, due to increase in resistivity, showed a negative MR of 3.5% at 25 K. To understand the origin of MR, all the data were fit by the equation originally developed by Khosla *et al.*[19]

$$\frac{\Delta R}{R_0} = -a^2 \ln(1+b^2B^2) + \frac{(c^2B^2)}{(1+d^2B^2)}, \qquad (1)$$

where B is the magnetic field, $B=\mu H$. The negative part in Eq. (1) is described by spin scattering that takes in to account

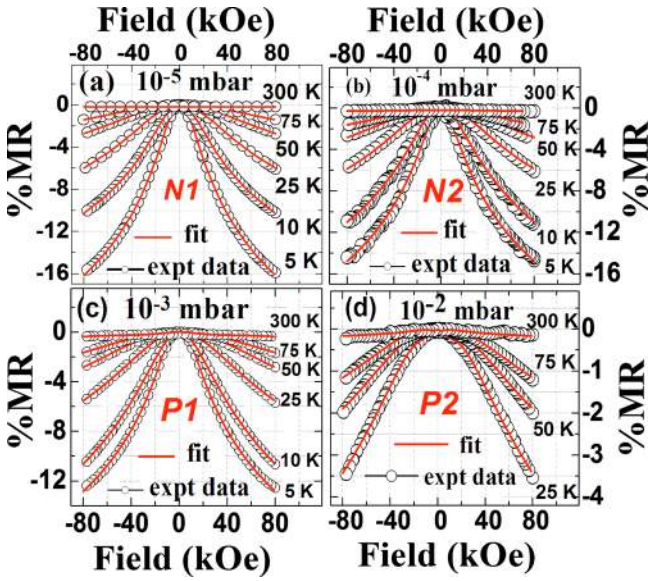

FIG. 3. (Color online) MR of the (a) *N*1 (n-type), (b) *N*2 (n-type), (c) *P*1 (p-type), and (d) *P*2 (p-type) Li–Ni codoped ZnO thin films. Circle represents the experimental data and the solid line represents least square fit.

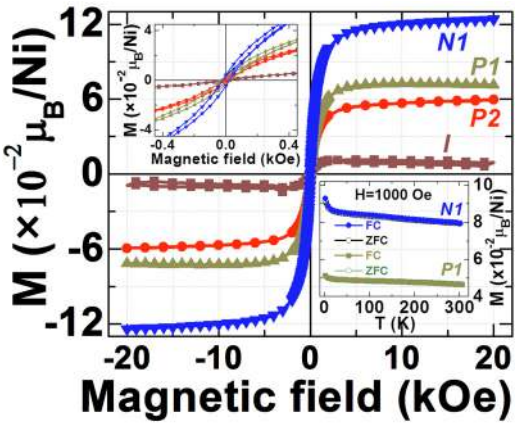

FIG. 4. (Color online) Room temperature *M-H* curves of the n-type, p-type, and insulating Li–Ni codoped ZnO thin films. Top inset shows the low field magnetization data depicting clear hysteresis loops. Bottom inset shows the temperature dependent magnetization (*M-T*) measurements of *N*1 and *P*1 thin films.

of the third-order expansion of the *s-d* exchange Hamiltonian while the positive part can be obtained from the two-band model. The fitting parameters a and b are given by,

$$a^2 = A_1 J \rho_F [S(S+1) + \langle M^2 \rangle]$$

$$\text{and} \quad b^2 = \left[1 + 4S^2\pi^2\left(\frac{2J\rho_F}{g}\right)^4\right]\frac{g^2\mu^2}{(\alpha kT)^2},$$

where A_1 is the measure of spin based scattering, $\langle M \rangle$ is the average magnetization, S is the spin of the localized moment, J is the exchange integral, ρ_F is the density of states at the Fermi energy, g is the g-factor, and α is a numerical constant. The parameters c and d are functions of conductivity and charge carrier concentrations. It is clear from the Fig. 4 that the least square fits are in good agreement with the experimental curves for all the samples. The fit parameter b has been found to decrease linearly with T as per theory[19] (not shown here). Moreover, the fitting parameter a decreases with increase in oxygen partial pressure revealing that the average magnetization declines at high oxygen partial pressures. Hence the negative MR may originate from the scattering of the charge carriers due to localized magnetic moments.

In order to understand the influence of oxygen vacancies, carrier concentration, and carrier type on the ferromagnetic ordering, we have carried out the magnetic measurements of the Li–Ni codoped ZnO thin films that showed n-type, p-type, and insulating behavior. Figure 4 shows the magnetization measurements (*M-H*) of the *N*1, *P*1, *P*2, and *I* samples. The insulating film (*I*) does not show any coercive field indicating superparamagnetic nature. However, both n-type (*N*1) and p-type (*P*1 and *P*2) films showed clear hysteresis loops (see inset of Fig. 4) at 300 K revealing room temperature ferromagnetism. Magnetization versus temperature (*M-T*) curves of the samples *N*1 and *P*1 clearly showed the Curie temperature is above 300 K. Very interestingly we have observed that the saturation magnetization (M_s) of the films strongly depends on the oxygen growth pressure and carrier concentration and not on the carrier type. The film *N*1, with $n=3.3\times10^{18}$ cm^{-3}, exhibited a maximum M_s of 0.12 μ_B/Ni. The films *P*1 ($p=8.2\times10^{17}$ cm^{-3}), *P*2 ($p=2.1\times10^{17}$ cm^{-3}), and *I* showed M_s of ~0.07 μ_B/Ni, 0.06 μ_B/Ni, and 0.009 μ_B/Ni, respectively. This clearly shows that the oxygen vacancies and carrier concentration play a crucial role in determining ferromagnetic ordering, which can be more suitably explained using defect mediated mechanism—the so called bound magnetic polaron (BMP) mechanism.[14] The exchange interaction between one localized carrier trapped by oxygen vacancies and many surrounding Ni ions align all the spins around the carrier localization center, forming BMP.[20] More the oxygen vacancies, greater the volume occupied by BMPs and hence large the probability of Ni ions overlapping that enhance the ferromagnetic ordering. Thus, Ni substitution in the zinc cation site and the oxygen vacancies may be jointly responsible for the observed ferromagnetism.

In summary, systematic thin film growth was undertaken to evolve n-type, p-type, and insulating ZnO. Electrical, magnetic, and magnetotransport studies of Li–Ni codoped ZnO suggest that both p-type conductivity and ferromagnetic ordering can be tuned by carefully controlling the oxygen vacancies. Moreover, our study clearly shows that the observed room temperature ferromagnetism has no dependence on the charge carrier type but solely depends on oxygen vacancies and the extent of carrier density.

The authors acknowledge Department of Science and Technology (DST) of India for the financial support (Grant No. SR/NM/NAT-02/2005).

[1]H. Zhu, C. X. Shan, B. Yao, B. H. Li, J. Y. Zhang, Z. Z. Zhang, D. X. Zhao, D. Z. Shen, X. W. Fan, Y. M. Lu, and Z. K. Tang, Adv. Mater. (Weinheim, Ger.) **21**, 1613 (2009).
[2]H. S. Kim, F. Lugo, S. J. Pearton, D. P. Norton, Y.-L. Wang, and F. Ren, Appl. Phys. Lett. **92**, 112108 (2008).
[3]M. Venkatesan, C. B. Fitzgerald, J. G. Lunney, and J. M. D. Coey, Phys. Rev. Lett. **93**, 177206 (2004).
[4]J. G. Lu, Y. Z. Zhang, Z. Z. Ye, L. P. Zhu, L. Wang, B. H. Zhao, and Q. L. Liang, Appl. Phys. Lett. **88**, 222114 (2006).
[5]A. Tsukazaki, A. Ohtomo, T. Onuma, M. Ohtani, T. Mahino, M. Sumiya, K. Ohtani, S. F. Chichibu, S. Fuke, Y. Segawa, H. Ohno, H. Koinuma, and M. Kawasaki, Nature Mater. **4**, 42 (2005).
[6]Z. Jin, T. Fukumura, M. Kawazaki, K. Ando, H. Saito, T. Sekiguchi, Y. Z. Yoo, M. Murakami, Y. Matsumoto, T. Hasegawa, and H. Koinuma, Appl. Phys. Lett. **78**, 3824 (2001).
[7]Z. Lu, H. S. Hsu, Y. Tzeng, and J. C. A. Huang, Appl. Phys. Lett. **94**, 152507 (2009).
[8]M. Gacic, H. Adrian, and G. Jakob, Appl. Phys. Lett. **93**, 152509 (2008).
[9]G. H. Ji, Z. B. Gu, M. H. Lu, D. Wu, S. T. Zhang, Y. Y. Zhu, S. N. Zhu, and Y. F. Chen, J. Phys.: Condens. Matter **20**, 425207 (2008).
[10]V. K. Sharma and G. D. Varma, J. Appl. Phys. **105**, 07C510 (2009).
[11]T. Dietl, H. Ohono, F. Matsukara, J. Cubert, and D. Ferrand, Science **287**, 1019 (2000).
[12]M. Khalid, M. Ziese, A. Setzer, P. Esquinazi, M. Lorenz, H. Hochmuth, M. Grundmann, D. Spemann, T. Butz, G. Brauer, W. Anwand, G. Fischer, W. A. Adeagbo, W. Hergert, and A. Ernst, Phys. Rev. B **80**, 035331 (2009).
[13]K. Sato and H. Katyama-Yoshida, Semicond. Sci. Technol. **17**, 367 (2002).
[14]J. M. D. Coey, M. Venkatesan, and C. B. Fitzgerald, Nature Mater. **4**, 173 (2005).
[15]M. Venkatesan, C. B. Fitzgerald, and J. M. D. Coey, Nature (London) **430**, 630 (2004).
[16]F. X. Xiu, Z. Yang, L. J. Mandalapu, and J. L. Liu, Appl. Phys. Lett. **88**, 152116 (2006).
[17]S. Ramachandran, J. Narayan, and J. T. Prater, Appl. Phys. Lett. **88**, 242503 (2006).
[18]G. Xing, D. Wang, J. Yi, L. Yang, M. Gao, M. He, J. Yang, J. Ding, T. C. Sum, and T. Wu, Appl. Phys. Lett. **96**, 112511 (2010).
[19]R. P. Khosla and J. R. Fischer, Phys. Rev. B **2**, 4084 (1970).
[20]Z. L. Lu, H. S. Hsu, Y. H. Tzeng, F. M. Zhang, Y. W. Du, and J. C. A. Huang, Appl. Phys. Lett. **95**, 102501 (2009).